Journal of Biomechanics 42 (2009) 2279–2285

Contents lists available at ScienceDirect

Journal of Biomechanics

journal homepage: www.elsevier.com/locate/jbiomech
www.JBiomech.com

Measurement of local strains in intervertebral disc anulus fibrosus tissue under dynamic shear: Contributions of matrix fiber orientation and elastin content

Arthur J Michalek [a], Mark R Buckley [b], Lawrence J Bonassar [c], Itai Cohen [b], James C Iatridis [a,*]

[a] College of Engineering and Mathematical Sciences, University of Vermont, 201 Perkins Building, 23 Colchester Ave, Burlington, VT 05405, USA
[b] Department of Physics, Cornell University, Ithaca, NY, USA
[c] Department of Biomedical Engineering and Sibley School of Mechanical and Aerospace Engineering, Cornell University, Ithaca, NY, USA

ARTICLE INFO

Article history:
Accepted 17 June 2009

Keywords:
Intervertebral
Disc
Shear
Confocal

ABSTRACT

Shear strain has been implicated as an initiator of intervertebral disc anulus failure, however a clear, multi-scale picture of how shear strain affects the tissue microstructure has been lacking. The purposes of this study were to measure microscale deformations in anulus tissue under dynamic shear in two orie ntations, and to determine the role of elastin in regulating these deformations. Bovine AF tissue was simultaneously shear loaded and imaged using confocal microscopy following either a buffer or elastase treatment. Digital image analysis was used to track through time local shear strains in specimens sheared transversely, and stretch and rotation of collagen fiber bundles in specimens sheared circumferentially. The results of this study suggest that sliding does not occur between AF plies under shear, and that interlamellar connections are governed by collagen and fibrilin rather than elastin. The transverse shear modulus was found to be approximately 1.6 times as high in plies the direction of the collagen fibers as in plies across them. Under physiological levels of in-plane shear, fiber bundles stretched and re-oriented linearly. Elastin was found to primarily stiffen plies transversely. We conclude that alterations in the elastic fiber network, as found with IVD herniation and degeneration, can therefore be expected to significantly influence the AF response to shear making it more susceptible to micro failure under bending or torsion loading.

1. Introduction

Acute injury and age related degeneration of the intervertebral disc (IVD) result in disruption of the anulus fibrosus (AF) structure, which is slow to repair due to its avascular nature and low cell density. Maintaining the integrity of the AF structure is crucial to long-term health and function of the IVD, and greater knowledge of AF micromechanics is essential to improve understanding IVD pathophysiology and modeling. The AF is a complex structure made up of unidirectional plies composed primarily of Types I and II collagen arranged in layers with alternating fiber orientations. Anular plies are interconnected through a hierarchical network of smaller fibers involving interactions between aggrecan, versican, fibrilin, elastin, and lubricin (Sherratt et al., 2003; Akhtar et al., 2005; Shine and Spector, 2008).

Shear is an important loading mode in the AF particularly relevant under bending and torsion loading of the IVD. The value of maximum shear strain (a potential failure criteria) in the IVD is largest in the AF under flexion–extension and lateral bending during physiological motions (Costi et al., 2007). For example, excessive flexion has long been implicated in acute IVD injury (Adams and Hutton, 1981; Adams and Roughley, 2006), suggesting that tissue level shear strains may be directly responsible for microstructural damage. Shear is mechanism for microscale failure initiation in all fiber reinforced composite materials, and is a likely initiator of AF failure (Iatridis and ap Gwynn, 2004). Bulk shear properties of AF explants have been investigated demonstrating anisotropic mechanical behaviors that are affected by degeneration (Iatridis et al., 1999; Fujita et al., 2000), however, there is no clear understanding of how tissue scale shear strains in the IVD are translated to fiber scale shear strains. Establishing this link is necessary for defining structural failure mechanisms and also for understanding cell–tissue mechanotransduction under healthy and degenerated conditions.

There is limited understanding of the strength of AF interlamellar interactions (Pezowicz et al., 2006), yet weak interactions have been proposed to contribute to IVD herniation (Veres et al., 2008). Interlamellar sliding has been proposed as a principal

* Corresponding author. Tel.: +1 802 656 2774; fax: +1 802 656 1929.
E-mail address: james.iatridis@uvm.edu (J.C. Iatridis).

0021-9290/$ - see front matter © 2009 Elsevier Ltd. All rights reserved.
doi:10.1016/j.jbiomech.2009.06.047

deformation mechanism in the AF (Szirmai, 1970; Broberg and von Essen, 1980; Broberg, 1983), and this notion is reinforced by the knowledge that plies may be separated via blunt dissection (Skaggs et al., 1994; Holzapfel et al., 2005). When interlamellar connections are ignored, modeling work (Guerin and Elliott, 2007) has shown discrepancies with experimental data, suggesting that these connections play a structurally significant role.

A comprehensive multi-scale understanding of AF tissue remains an important gap in the literature, although much information on AF mechanics is known on different scales. Single plies of AF tissue have been measured (Skaggs et al., 1994; Holzapfel et al., 2005), and AF lamellar mechanics are affected by alterations in fiber orientation, matrix and fiber properties, and interactions between matrix constituents (Elliott and Setton, 2001; Wagner and Lotz, 2004; Guerin and Elliott, 2007). AF fiber tension plays an important role restricting axial rotation of the IVD (Krismer et al., 1996), and AF fiber strains were 6% or less under physiological loading (Stokes, 1987). Confocal microscopy of whole bovine IVDs under flexion determined that interfibrillar sliding occurs producing large shear strains on the cells (Bruehlmann et al., 2004a, b). This study by Bruehlmann and co-authors provided novel multi-scale information on AF mechanics with particular focus how IVD loading influences cell mechanics. However, there remains a lack of information on how AF tissue shearing impacts interlamellar and fibrillar mechanics including fiber orientation, fiber crimp, and tissue stiffness.

The role of elastin in AF mechanics is of emerging interest (Smith and Fazzalari, 2009) and this role is expected to change with degeneration. Elastin proteins assemble into a sparse network of highly extensible elastic fibers. Accounting for approximately 2% of tissue dry weight (Mikawa et al., 1986; Olczyk, 1994; Cloyd and Elliott, 2007), and the precise structural role of elastic fibers has only recently been explored (Smith et al., 2008). Age related degeneration is correlated with an increase in elastin content relative to tissue dry weight (Cloyd and Elliott, 2007), and a visible decrease in intact elastic fibers (Johnson et al., 1985), suggesting that breakdown and synthesis of elastic fibers may be an important structural remodeling process. Disc prolapse has been linked with increased elastin content (Olczyk, 1994) and increased enzymatic activity against elastin (Ng et al., 1986). Disorganization in the IVD's elastic fiber network has also been observed as a result of both idiopathic and neuromuscular scoliosis (Akhtar et al., 2005; Yu et al., 2005). Disruption of this network under disc bending conditions, which generate high shear strains, suggests that elastic fibers play an important role in microscale shear mechanics of the AF.

The present study measured microscale deformations in bovine AF tissue under shear in transverse and circumferential orientations (Fig. 1) in both the healthy state and with a disrupted elastin network. We hypothesized that: (1) transverse shear deformation results from intralamellar skewing in healthy tissue and that elastase digestion will also allow interlamellar sliding and (2) circumferential shear results from independent mechanisms of stretch and rotation of collagen fiber bundles and that disruption of interlamellar connectivity through elastase digestion will reduce fiber strain and increase fiber rotation. These hypotheses were tested using simultaneous dynamic shear loading and confocal microscopy followed by digital image analyses to measure microscale deformations.

2. Materials and methods

2.1. Specimen preparation

Twenty-four AF specimens were taken from caudal levels 2–3 through 5–6 of the tails of two skeletally mature steers within 24 h of sacrifice. Each anulus was divided into four quadrants, and each quadrant was assigned to one of four groups defined by combinations of elastase treatment (digested or control) and specimen orientation (transverse or circumferential as shown in Fig. 1). Specimens were systematically grouped such that each treatment received the same number of specimens from each anatomical region; anterior, posterior, and lateral. Following rough dissection, specimens were soaked for 36 h in either tris buffer (pH 6.8), or tris buffer with porcine pancreatic elastase (Sigma). Benzamadine (0.75 mg/mL) and *N*-ethylmaleimide (1.25 mg/mL) were added to both solutions as protease inhibitors. After soaking, a cryostat cut tissues into ~5 mm cubes, with care taken to maintain parallel faces. Exact cube dimensions were recorded, specimens were wrapped in PBS soaked gauze and stored at −20 °C until testing.

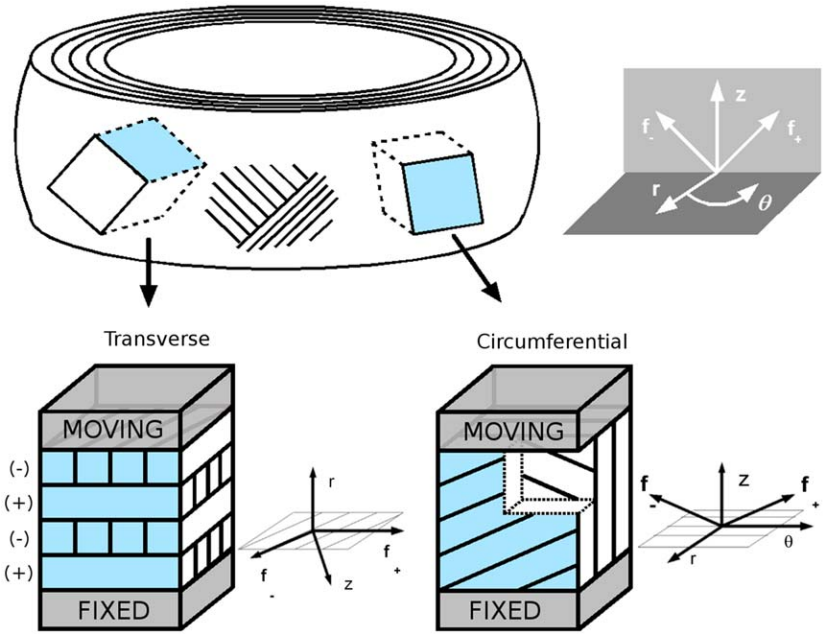

Fig. 1. Specimen orientations with imaged faces shaded (top). Boundary conditions and coordinates (bottom). Transverse specimens were oriented such that the radial direction was vertical, ply boundaries were horizontal, and alternating plies were aligned either tangentially to the viewing plane (+) or approximately normal to the viewing plane (−). Circumferential specimens were oriented with the viewing plane parallel with the outside surface of the AF.

Prior to testing, cube specimens were thawed at room temperature, stained with 5-DTAF (4 mg/mL of DMSO) (Invitrogen) for 30 min, and rinsed in PBS for 30 min. DTAF was selected for uniform binding to all proteins in the tissue and resistance to photo-bleaching, which is ideal for emphasizing AF small scale tissue morphology (Bruehlmann et al., 2004a, b; Krahn et al., 2006).

2.2. Shear testing

Tissue specimens were tested in shear using a Harrick Scientific Tissue Deformation Imaging Stage (Buckley et al., 2008). Specimens were glued to the grips with cyanoacrylate, compressed to 90% of the specimen height measured, and allowed to reach force equilibrium while immersed in PBS. Compressive and tensile strains of 10% are within physiological limits in both transverse and circumferential orientations (Tsantrizos et al., 2005). Sinusoidal shear deformation was then applied at $\pm 5\%$ of initial height and frequency of 50 mHz. The frequency was chosen to have a period significantly shorter than the shear relaxation time of AF tissue, reported as 20 min (Fujita et al., 2000). Five percent circumferential shear strain corresponds to approximately 1.7° torsion in human lumbar IVDs, well within normal physiological limits (Krismer et al., 1996), and 5% transverse shear corresponds to $\sim 1^\circ$ of lateral bending (Costi et al., 2007). Images of the tissue were captured during testing (Zeiss LSM 5 Live inverted confocal microscope) at a rate of 15 frames per second. The shear tests were then repeated at 100% and 110% of the specimen's original height with force equilibrium reached prior to each shear test.

2.3. Image analysis

Digital analysis was performed to calculate microscale strains based on the images obtained by confocal microscopy. For the transverse experiment, particle image velocimetry (PIV) was used to track shear strain in time within a rectangular region of interest (ROI). For the circumferential experiment, two-dimensional cross correlation was used to track pairs of points located along a collagen fiber bundle to measure stretch and rotation. Both analyses began with a processing routine to reduce the grayscale images to binary images of particle-like features, a time series process, and a calculation of dependent variables.

Image processing for both transverse and circumferential tests was performed using custom software written in Matlab (Mathworks, Natick, MA). After each raw image (Figs. 2a, c and d) was imported, intensity gradients resulting from imaging artifacts were flattened, the contrast of the image was stretched to use the entire intensity scale, and a modified Sobel filter was used to enhance feature edges. The image was then converted from grayscale to binary and inverted and a 2×2 pixel median filter removed random noise (Figs. 2b and d).

Microscale shear strains in transverse specimens were measured using PIV and performed in Matlab (mpiv toolbox by Nobuhito Mori, distributed under GNU public license). To reduce numerical bias resulting from variations in horizontal translation (which varies with the location of the imaging window relative to the boundaries of the specimen), the image series were down-sampled to between 1.5 and 2.5 frames per second. This step was performed to ensure that the average feature displacement between frames was approximately equal for all series, and thus numerical round off error had the same effect on analysis of all specimens. The PIV routine was run using the correlation algorithm with an average 15 pixel square window, a 3 pixel overlap, and a unit time step. Following velocimetry measurements, the resulting series of vector fields was stored.

Local shear strain was measured by drawing a rectangular ROI on the first frame of the image series, which was then filled in with a uniformly spaced grid. At each time step, the two-dimensional velocity field was interpolated cubically to the grid vertices, which were then moved by the velocity multiplied by the length of the time step. The shear strain of each grid square was calculated, and the average of all grid squares recorded. An example ROI grid in unstrained and strained states is shown (Figs. 3a and b). A sine function was fit to the recorded shear strains, and used to determine the shear strain amplitude of the ROI as well as its phase angle relative to the applied strain. A typical local shear strain trace with sine fit is shown (Fig. 3c). This analysis was performed for three-different ROIs each in adjacent plies of different orientations. Since the absolute value of phase angle was dependent on the ROI's location between the fixed and moving platens, the phase angle of each ROI from a $(-)$ ply was divided by the phase angle of an ROI in an adjacent (+) ply to provide a measure of relative viscoelasticity.

Fiber stretch and re-orientation were measured in circumferential specimens by tracking through the image series the endpoints of a line drawn along the fiber orientation on the first frame. For each of the line's endpoints, a small sub-image containing surrounding features was stored and compared to the next frame by computing the two-dimensional cross-correlation function between the two images, and repeated throughout the image series. Fig. 3 shows a pair of frames from a typical circumferential image series showing the unstrained (d) and strained (e) states. Following tracking, the locations of the two points were used to calculate the length and angular orientation of the line versus time (Fig. 3f).

Prior to analysis, both routines were validated by performing them on binary image sets with known displacements applied to the features. As a quality control measure, ROI strain (transverse experiment) or fiber stretch (circumferential experiment) were recorded only when the mesh vertices or tracking points returned to their original positions following a full cycle of shearing.

A continuous fiber connecting two parallel surfaces which are translating relative to each other will stretch and rotate under cyclic shear with an amplitude which depends on its initial angle of orientation (Fig. 4). To reduce the effect of interspecimen variability resulting from differences in initial collagen fiber orientation, measured stretch and rotation were normalized based on theoretical

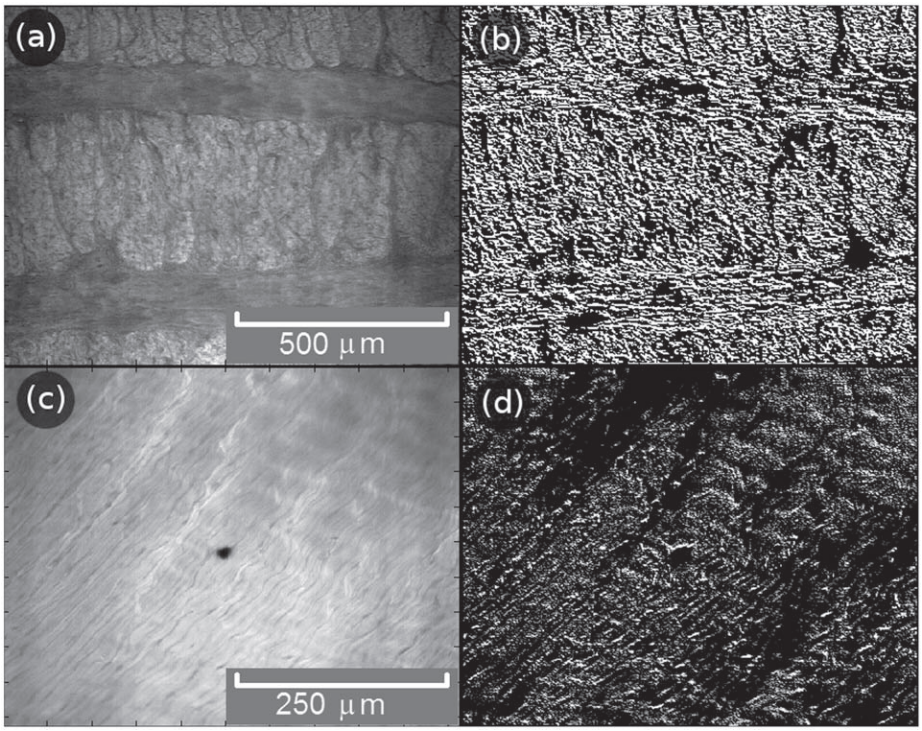

Fig. 2. Processing for typical transverse (a–b) and circumferential (c–d) images, showing raw images (a, c), normalized, contrast stretched, and edge filtered (b, d).

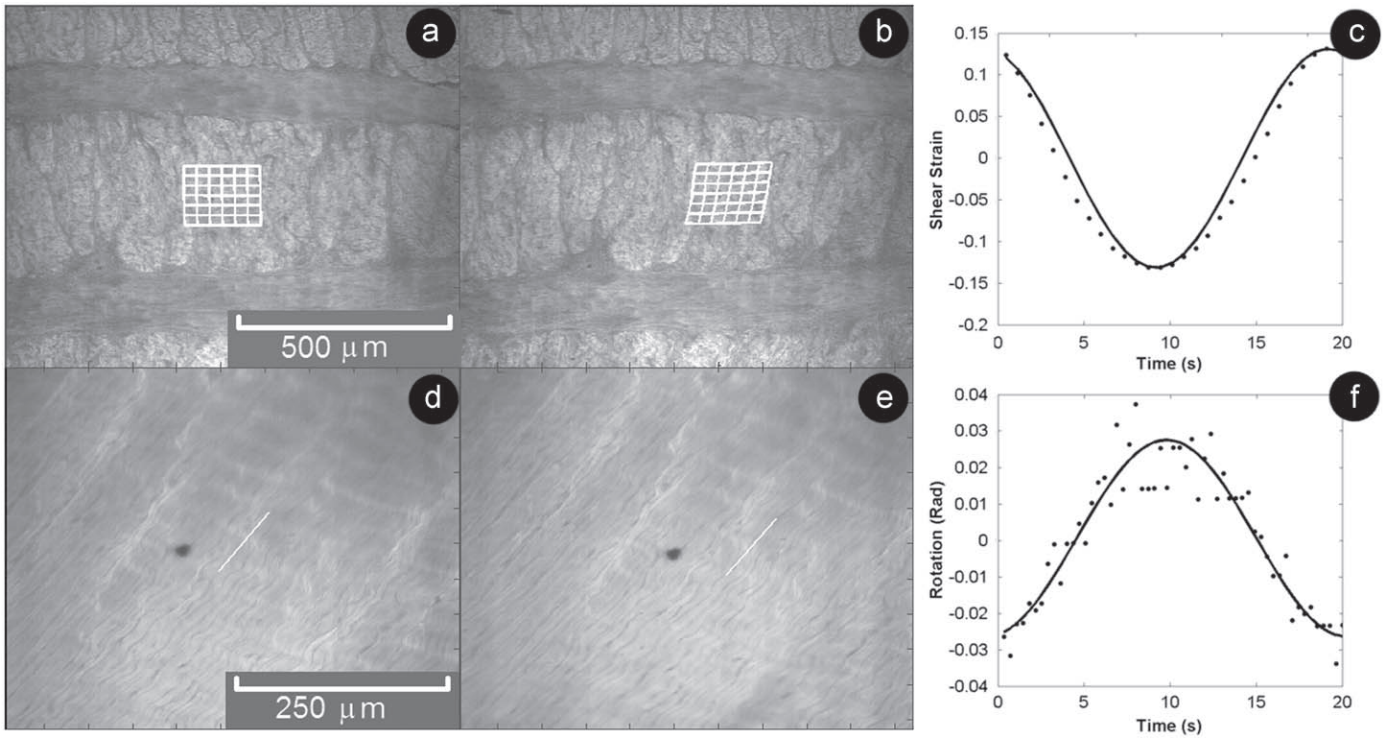

Fig. 3. Typical transverse (a–c) and circumferential (d–f) images in the unstrained (a, d) and strained (b, e) states. Though processed images as shown in Fig. 2 (c, f) were used for calculations, the results have been projected onto raw confocal images to more clearly show tissue morphology. Traces of calculated local shear strain (c) and fiber rotation (f) are shown measured, ●, over one shear cycle with sine function fit, –.

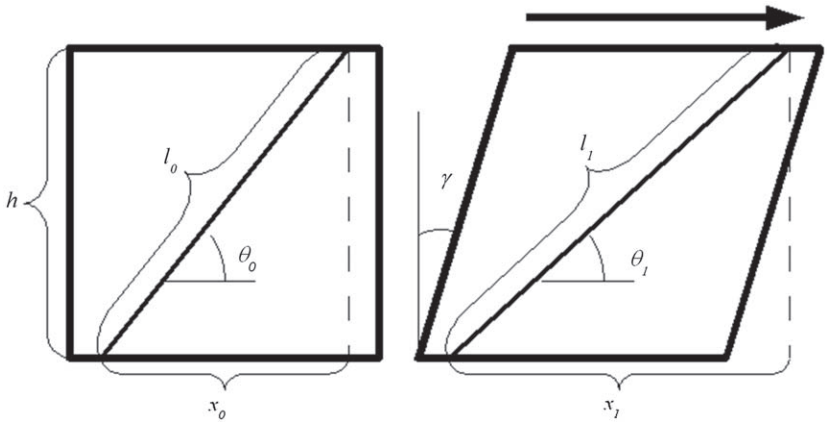

Fig. 4. Geometric representation of stretch and re-orientation of a line drawn obliquely on the surface of a continuous solid under shear.

estimates. The estimates assumed small strain, no edge effects, and no compressibility. They yielded the following expressions for stretch, l^*, and rotation, θ, amplitudes depending on average angle of orientation, θ_0, and far-field strain amplitude, γ. Derivations of Eqs. (1) and (2) are provided in the supplemental materials.

$$\theta^* = 2\left|\tan^{-1}\left(\left[\left(\frac{1}{\tan\theta_0}\right)+\tan\gamma\right]^{-1}\right)-\theta_0\right| \quad (1)$$

$$l^* = 2\left|\left[(\cos(\theta_0)+\sin(\theta_0)\tan(\gamma))^2+\sin^2(\theta_0)\right]^{1/2}-1\right| \quad (2)$$

2.4. Statistics

Three way ANOVA measured effects of elastase treatment, ply orientation, and radial strain on intralamellar local shear strain amplitude data from transverse shear tests. Two way ANOVA measured effects of elastase treatment and axial strain on normalized fiber strain and rotation data from circumferential shear tests. Paired *t*-tests with Bonferonni correction were used for post-hoc comparisons. All normalized results were also compared to unity to test the hypothesis that they matched the theoretical predictions. Statistical tests were performed in Matlab using $p<0.05$ as significant.

2.5. Histology

Histological analysis using Orcein was performed on both control and digested tissue specimens to evaluate the effectiveness of the elastase treatment, and to visualize the elastic fiber structure in the transverse plane. Slices of 20 μm thickness were cut from frozen AF samples using a cryostat and stored on Polysine (Esco, Portsmouth, NH) coated glass slides at −20 °C until staining. Sections were re-hydrated with PBS, then treated overnight with hyaluronidase (4800 U/mL in PBS) to remove proteoglycans, and for 4 h with collagenase (30 U/mL in PBS with 1 mM $MCaCl_2$) to remove collagen. Following digestion, the sections were rinsed with 70% ethanol and stained for 45 min with Orcein (1%+1% concentrated HCl in 80% ethanol). Following staining, sections were rinsed twice with 70% ethanol, then dehydrated via serial ethanol rinses at 70%, 90%, and 100%. Cover slips were mounted, and specimens were imaged under bright field.

3. Results

Intralamellar shear strains observed in the transverse experiment showed significant effects of elastase treatment and ply orientation along with a significant interaction. In general, strain in normally oriented (−) plies were significantly higher than the applied 5%, and strain in the tangentially oriented (+) plies were significantly lower (Fig. 5). In all cases, strain was higher in (−) plies than in (+) plies. Elastase treatment significantly increased strain in (−) plies under all radial strain conditions. Radial strain magnitude had no significant effect on local strain amplitudes. While not significant, elastase treatment increased both magnitude and variance of the ratio of (−) phase angle to (+) phase angle.

Micrographs of control specimens in the transverse orientation (Fig. 6) showed elastic fibers concentrated around collagen fiber bundles and randomly oriented. Elastic fibers located along ply boundaries were radially oriented. Localized concentrations of radially oriented elastic fibers also spanned multiple plies in sparsely distributed cross bridge structures (Melrose et al., 2008; Schollum et al., 2008). No elastic fibers were visible in micrographs of elastase treated tissue.

In the circumferential experiment, normalized stretch and rotation were generally not significantly affected by elastase treatment or axial strain amplitude (Fig. 7). However, digested samples had significantly less fiber strain and significantly more fiber rotation under −10% and 0% axial strain than the theoretical predictions (i.e., compared to 1).

4. Discussion

Microscale strains in healthy and elastase treated AF tissue under dynamic shear were measured with a novel imaging stage mounted on a confocal microscope. Images were analyzed using PIV to obtain intralamellar strain in transversely oriented specimens, and using feature tracking to obtain fiber stretch and rotation in circumferentially oriented specimens. Deformation behaviors may be envisioned as several independent mechanisms (Fig. 8). Transverse shear has been thought to result from sliding along ply boundaries with some contribution of intralamellar skewing. Circumferential shear is believed to result from stretching and uncrimping of collagen fiber bundles combined with fiber bundle rotation. The present study directly observed these mechanisms with a minimal amount of disruption to the interlamellar connectivity of the AF structure, and provides new insight into the nature of this tissue structure.

The most significant finding of this study is that microscale deformation under transverse shear is solely the result of intralamellar skewing, the relative magnitude of which depends on a particular ply's orientation relative to the direction of applied shear. Anular plies do not slide relative to one another under shear even following elastase treatment. Based on the relative strain amplitudes in (+) and (−) plies, we estimate that the shear modulus of an individual ply of the AF is approximately 1.6 times as high along the fiber bundles as it is across them. Furthermore, the lack of observed sliding under radial tension indicates that the boundary interaction is governed by a rigid fibrous connection,

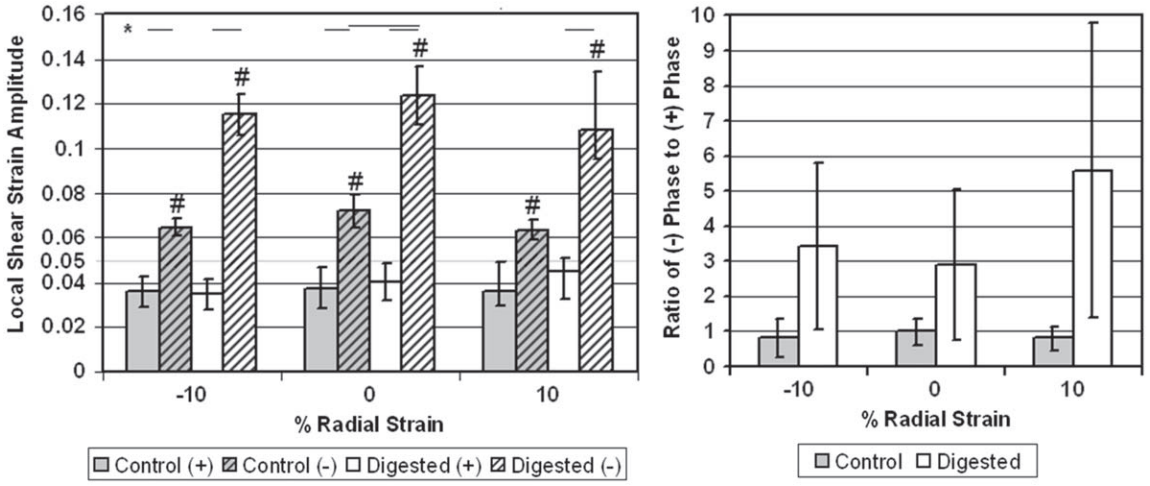

Fig. 5. Average local strain amplitude (left) and local phase ratio (right) ±SD for transverse tests. *: $p<0.05$ between groups and #: $p<0.05$ between average and applied shear.

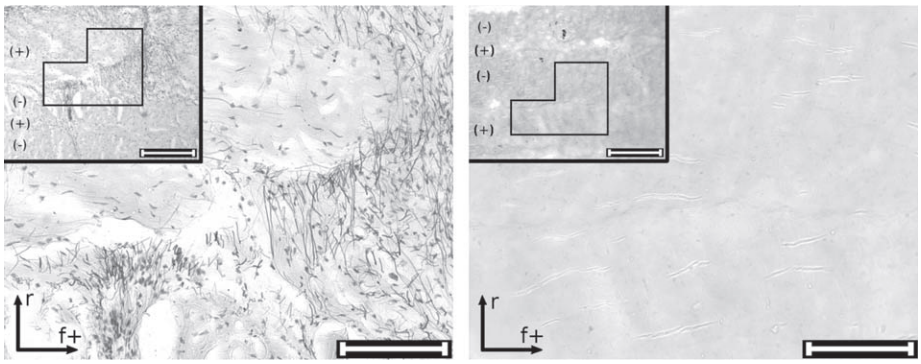

Fig. 6. Representative micrographs for orcein stained tissue in the transverse orientation. Control is shown left and digested right. Scale bars are 100 μm.

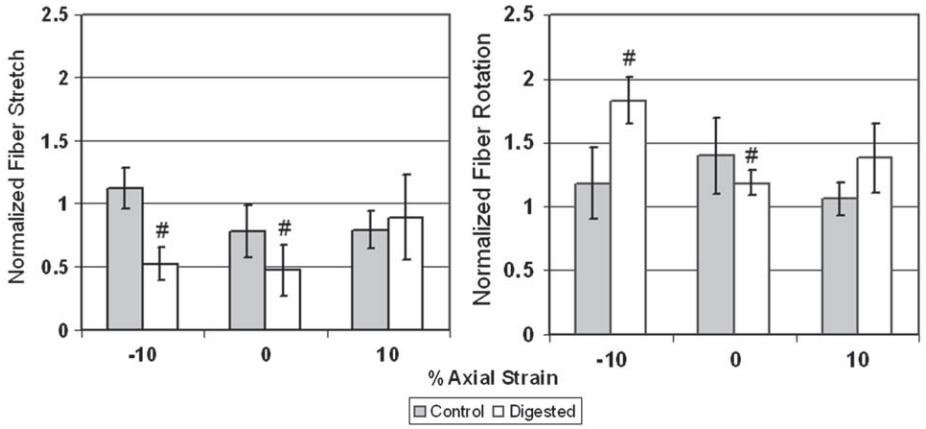

Fig. 7. Average fiber strain (left) and average fiber rotation (right) ±SD for circumferential tests *: $p<0.05$ between groups and #: $p<0.05$ between average and one.

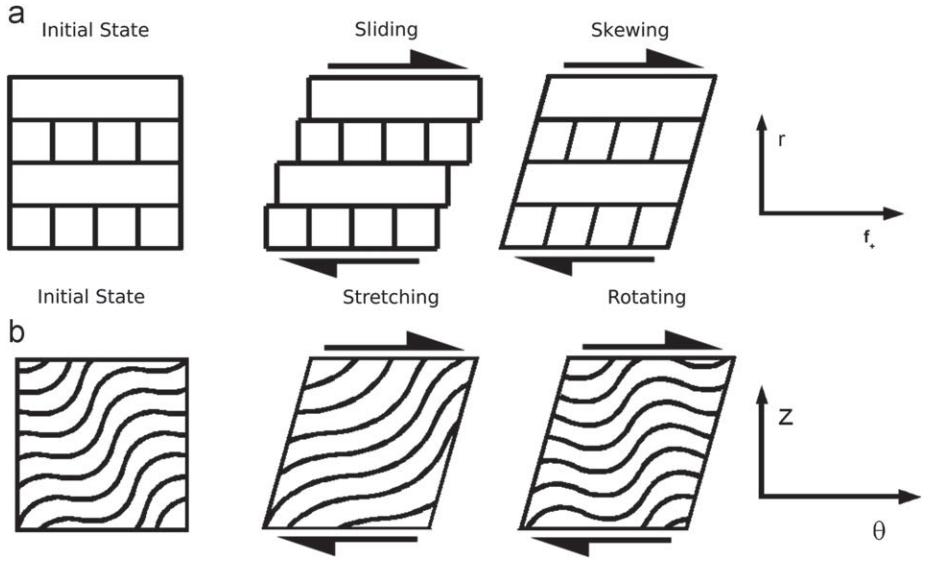

Fig. 8. Possible deformation modes of AF tissue under shear. Transverse shear is believed to result in a combination of interlamellar sliding and intralamellar skewing. Circumferential shear results in stretching and uncrimping in the collagen fiber bundle direction and rotation of the fiber bundles.

rather than surface to surface friction. This finding is in strong agreement with previous investigation into the radial tension in the AF (Pezowicz et al., 2006), which concluded that fibrous networks provide strong connectivity between adjacent plies. Surprisingly, despite the increased concentration of elastic fibers along interlamellar boundaries, they do not appear to play a significant role in boundary mechanics under shear. Rather, the elastic fiber network appears to contribute to the stiffness of the ply perpendicular to the collagen fiber bundle direction under transverse shear. The observed increase in relative phase angle between (−) and (+) plies in elastase treated specimens, combined with the change in relative stiffness, indicates that elastin also plays a role in orthotropic damping properties of anular plies.

The theoretical predictions of fiber stretch and rotation in the circumferential experiment assumed small deformations and no strain variations throughout the thickness of the specimen. These assumptions were shown to be valid for 5% applied strain amplitude in healthy tissue. Fiber uncrimping and re-orientation were also observed to occur simultaneously and continuously in all specimens, rather than as independent mechanisms. These observations indicate that interlamellar connections are sufficiently rigid to treat the structure as a continuous material under circumferential shear. Given our observation of decreased ply shear stiffness normal to fiber orientation following elastase treatment, the most likely cause of the observed deviation of stretch and rotation from the theoretical predictions in digested specimens under 0% and −10% axial strain is out of plane rotation in the ply being imaged.

The image analysis techniques used in this study are among the most robust available, yet the results are subject to some practical limitations. Due to the level of magnification, the PIV technique was most robust when the region of interest was centered within the middle three fourths of the ply. ROIs were selected accordingly, and as a result, strains in areas immediately adjacent to ply boundaries were not measured. It should be expected that the average of the local shear strains in the (+) and (−) plies for a given enzyme treatment and magnitude of radial strain (Fig. 5) be equal to the applied strain of 0.05. While this was the case for the control groups, it was not for the digested groups. It is thus possible that elastase treatment resulted in a decrease in shear stiffness near the center plane of the ply while the boundary area remained unaffected. It should also be noted that the images taken in this study are primarily of tissue from approximately 1–2 mm from the outer surface of the disc, and it is likely that variations in ply thickness and distributions of Types I and II collagen result in slightly different shear stiffness anisotropy from

the inner through outer AF. Though this study was limited by the use of bovine tail discs, bovine AF tissue has previously been shown to have water, proteoglycan, and Type II collagen content (Demers et al., 2004), as well as elastic fiber structure (Yu et al., 2005) similar to young adult human.

5. Conclusion

Local strains in the transverse direction were solely the result of intralamellar skewing even under elastase treatment. We conclude that sliding does not occur between AF layers, and that interlamellar connections may involve greater numbers of molecular interactions than previously thought. Importantly, elastin was found to have a specific mechanical role to stiffen the AF fiber bundles in transverse shear and to contribute to the anisotropy of the AF tissue shear stiffness. Elastase treatment allowed greater amounts of fiber rotation and significantly altered the tissue load carriage mechanisms under shear loading. Alterations in the elastic fiber network, as found with IVD herniation and degeneration, can therefore be expected to significantly influence the AF response to shear making it more susceptible to micro failure under motions which generate high tissue shear strains, such as bending or torsion.

Conflict of interest statement

The authors of this paper have no financial or personal conflicts which may bias the results presented. Funding in the form of research grants has been provided by the National Institute of Health: 1R01AR051146 and R21AR054867, The Vermont Space Grant Consortium: NNX07AK92A, and the National Science Foundation: DMR-0606040.

Acknowledgments

This work was funded by NIH: 1R01AR051146 and R21AR054867, NASA/VSGC: NNX07AK92A, and NSF: DMR-0606040.

Appendix. Supporting information

Supplementary data associated with this article can be found in the online version at doi:10.1016/j.jbiomech.2009.06.047.

References

Adams, M.A., Hutton, W.C., 1981. The relevance of torsion to the mechanical derangement of the lumbar spine. Spine 6 (3), 241–248.
Adams, M.A., Roughley, P.J., 2006. What is intervertebral disc degeneration, and what causes it?. Spine 31 (18), 2151–2161.
Akhtar, S., Davies, J.R., et al., 2005. Ultrastructural immunolocalization of alpha-elastin and keratan sulfate proteoglycan in normal and scoliotic lumbar disc. Spine 30 (15), 1762–1769.
Broberg, K.B., 1983. On the mechanical behaviour of intervertebral discs. Spine 8 (2), 151–165.
Broberg, K.B., von Essen, H.O., 1980. Modeling of intervertebral discs. Spine 5 (2), 155–167.
Bruehlmann, S.B., Hulme, P.A., et al., 2004. In situ intercellular mechanics of the bovine outer annulus fibrosus subjected to biaxial strains. J. Biomech. 37 (2), 223–231.
Bruehlmann, S.B., Matyas, J.R., et al., 2004. ISSLS prize winner: collagen fibril sliding governs cell mechanics in the anulus fibrosus: an in situ confocal microscopy study of bovine discs. Spine 29 (23), 2612–2620.
Buckley, M.R., Gleghorn, J.P., et al., 2008. Mapping the depth dependence of shear properties in articular cartilage. J. Biomech. 41 (11), 2430–2437.
Cloyd, J.M., Elliott, D.M., 2007. Elastin content correlates with human disc degeneration in the anulus fibrosus and nucleus pulposus. Spine 32 (17), 1826–1831.
Costi, J.J., Stokes, I.A., et al., 2007. Direct measurement of intervertebral disc maximum shear strain in six degrees of freedom: motions that place disc tissue at risk of injury. J. Biomech. 40 (11), 2457–2466.
Demers, C.N., Antoniou, J., et al., 2004. Value and limitations of using the bovine tail as a model for the human lumbar spine. Spine 29 (24), 2793–2799.
Elliott, D.M., Setton, L.A., 2001. Anisotropic and inhomogeneous tensile behavior of the human anulus fibrosus: experimental measurement and material model predictions. J. Biomech. Eng. 123 (3), 256–263.
Fujita, Y., Wagner, D.R., et al., 2000. Anisotropic shear behavior of the annulus fibrosus: effect of harvest site and tissue prestrain. Med. Eng. Phys. 22 (5), 349–357.
Guerin, H.L., Elliott, D.M., 2007. Quantifying the contributions of structure to annulus fibrosus mechanical function using a nonlinear, anisotropic, hyperelastic model. J. Orthop. Res. 25 (4), 508–516.
Holzapfel, G.A., Schulze-Bauer, C.A., et al., 2005. Single lamellar mechanics of the human lumbar anulus fibrosus. Biomech. Model Mechanobiol. 3 (3), 125–140.
Iatridis, J.C., ap Gwynn, I., 2004. Mechanisms for mechanical damage in the intervertebral disc annulus fibrosus. J. Biomech. 37 (8), 1165–1175.
Iatridis, J.C., Kumar, S., et al., 1999. Shear mechanical properties of human lumbar annulus fibrosus. J. Orthop. Res. 17 (5), 732–737.
Johnson, E.F., Berryman, H., et al., 1985. Elastic fibres in the anulus fibrosus of the adult human lumbar intervertebral disc. A preliminary report. J. Anat. 143, 57–63.
Krahn, K.N., Bouten, C.V., et al., 2006. Fluorescently labeled collagen binding proteins allow specific visualization of collagen in tissues and live cell culture. Anal. Biochem. 350 (2), 177–185.
Krismer, M., Haid, C., et al., 1996. The contribution of anulus fibers to torque resistance. Spine 21 (22), 2551–2557.
Melrose, J., Smith, S.M., et al., 2008. Aggrecan, versican and Type VI collagen are components of annular translamellar crossbridges in the intervertebral disc. Eur. Spine J. 17 (2), 314–324.
Mikawa, Y., Hamagami, H., et al., 1986. Elastin in the human intervertebral disk. A histological and biochemical study comparing it with elastin in the human yellow ligament. Arch. Orthop. Trauma Surg. 105 (6), 343–349.
Ng, S.C., Weiss, J.B., et al., 1986. Abnormal connective tissue degrading enzyme patterns in prolapsed intervertebral discs. Spine 11 (7), 695–701.
Olczyk, K., 1994. Changes in macromolecular components of prolapsed intervertebral discs. Ann. Biol. Clin. (Paris) 52 (10), 711–716.
Pezowicz, C.A., Robertson, P.A., et al., 2006. The structural basis of interlamellar cohesion in the intervertebral disc wall. J. Anat. 208 (3), 317–330.
Schollum, M.L., Robertson, P.A., et al., 2008. ISSLS prize winner: microstructure and mechanical disruption of the lumbar disc annulus: Part I: a microscopic investigation of the translamellar bridging network. Spine.
Sherratt, M.J., Baldock, C., et al., 2003. Fibrillin microfibrils are stiff reinforcing fibres in compliant tissues. J. Mol. Biol. 332 (1), 183–193.
Shine, K.M., Spector, M., 2008. The presence and distribution of lubricin in the caprine intervertebral disc. J. Orthop. Res. 26 (10), 1398–1406.
Skaggs, D.L., Weidenbaum, M., et al., 1994. Regional variation in tensile properties and biochemical composition of the human lumbar anulus fibrosus. Spine 19 (12), 1310–1319.
Smith, L.J., Byers, S., et al., 2008. Elastic fibers enhance the mechanical integrity of the human lumbar anulus fibrosus in the radial direction. Ann. Biomed. Eng. 36 (2), 214–223.
Smith, L.J., Fazzalari, N.L., 2009. The elastic fibre network of the human lumbar anulus fibrosus: architecture, mechanical function and potential role in the progression of intervertebral disc degeneration. Eur. Spine. J. 18 (4), 39–48.
Stokes, I.A., 1987. Surface strain on human intervertebral discs. J. Orthop. Res. 5 (3), 348–355.
Szirmai, J., 1970. Structure of the intervertebral disc. In: Balazs, E. (Ed.), Chemistry and Molecular Biology of the Intercellular Matrix, vol. 3. Academic Press, New York, pp. 1279–1308.
Tsantrizos, A., Ito, K., et al., 2005. Internal strains in healthy and degenerated lumbar intervertebral discs. Spine 30 (19), 2129–2137.
Veres, S.P., Robertson, P.A., et al., 2008. ISSLS prize winner: microstructure and mechanical disruption of the lumbar disc annulus: Part II: how the annulus fails under hydrostatic pressure. Spine.
Wagner, D.R., Lotz, J.C., 2004. Theoretical model and experimental results for the nonlinear elastic behavior of human annulus fibrosus. J. Orthop. Res. 22 (4), 901–909.
Yu, J., Fairbank, J.C., et al., 2005. The elastic fiber network of the anulus fibrosus of the normal and scoliotic human intervertebral disc. Spine 30 (16), 1815–1820.